ISSN 1674-1056
http://cpb.iphy.ac.cn
http://iopscience.iop.org/cpb
中国物理 B
Chinese Physics
中国物理 Chinese Physics B

Enhanced thermoelectric properties of p-type polycrystalline SnSe by regulating the anisotropic crystal growth and Sn vacancy

Chengyan Liu(刘呈燕), Lei Miao(苗蕾), Xiaoyang Wang(王潇漾), Shaohai Wu(伍少海), Yanyan Zheng(郑岩岩), Ziyang Deng(邓梓阳), Yulian Chen(陈玉莲), Guiwen Wang(王桂文), Xiaoyuan Zhou(周小元)
Citation: Chin. Phys. B . 2018, 27(4): 047211. **doi:** 10.1088/1674-1056/27/4/047211

Journal homepage: http://cpb.iphy.ac.cn; http://iopscience.iop.org/cpb

What follows is a list of articles you may be interested in

Enhanced thermoelectric performance in p-type Mg_3Sb_2 via lithium doping

Hao Wang(王浩), Jin Chen(陈进), Tianqi Lu(陆天奇), Kunjie Zhu(朱坤杰), Shan Li(李珊), Jun Liu(刘军), Huaizhou Zhao(赵怀周)
Chin. Phys. B . 2018, 27(4): 047212. **doi:** 10.1088/1674-1056/27/4/047212

Biaxial strain-induced enhancement in the thermoelectric performance of monolayer WSe_2

Wanhuizi Shen(沈婉慧子), Daifeng Zou(邹代峰), Guozheng Nie(聂国政), Ying Xu(许英)
Chin. Phys. B . 2017, 26(11): 117202. **doi:** 10.1088/1674-1056/26/11/117202

Thermoelectric properties of Li-doped $Sr_{0.7}Ba_{0.3}Nb_2O_{6-\delta}$ ceramics

Ya-Cui Zhang(张亚翠), Jian Liu(刘剑), Yi Li(李宜), Yu-Fei Chen(陈宇飞), Ji-Chao Li(李吉超), Wen-Bin Su(苏文斌), Yu-Cheng Zhou(周昱成), Jin-Ze Zhai(翟近泽), Teng Wang(王腾), Chun-Lei Wang(王春雷)
Chin. Phys. B . 2017, 26(10): 107201. **doi:** 10.1088/1674-1056/26/10/107201

Optimize the thermoelectric performance of CdO ceramics by doping Zn

Xin-Yu Zha(查欣雨), Lin-Jie Gao(高琳洁), Hong-Chang Bai(白洪昌), Jiang-Long Wang(王江龙), Shu-Fang Wang(王淑芳)
Chin. Phys. B . 2017, 26(10): 107202. **doi:** 10.1088/1674-1056/26/10/107202

Influences of spark plasma sintering temperature on the microstructures and thermoelectric properties of $(Sr_{0.95}Gd_{0.05})TiO_3$ ceramics

Li Liang-Liang, Qin Xiao-Ying, Liu Yong-Fei, Liu Quan-Zhen
Chin. Phys. B . 2015, 24(6): 067202. **doi:** 10.1088/1674-1056/24/6/067202

SPECIAL TOPIC — Recent advances in thermoelectric materials and devices

Enhanced thermoelectric properties of p-type polycrystalline SnSe by regulating the anisotropic crystal growth and Sn vacancy*

Chengyan Liu(刘呈燕)[1], Lei Miao(苗蕾)[1,†], Xiaoyang Wang(王潇漾)[1], Shaohai Wu(伍少海)[1], Yanyan Zheng(郑岩岩)[1], Ziyang Deng(邓梓阳)[1], Yulian Chen(陈玉莲)[1], Guiwen Wang(王桂文)[2], and Xiaoyuan Zhou(周小元)[2]

[1] *Guangxi Key Laboratory of Information Material, Guangxi Collaborative Innovation Center of Structure and Property for New Energy and Materials, School of Material Science and Engineering, Guilin University of Electronic Technology, Guilin* 541004, *China*

[2] *College of Physics, Chongqing University, Chongqing* 401331, *China*

(Received 1 March 2018; revised manuscript received 19 March 2018; published online 29 March 2018)

Thermoelectric selenides have attracted more and more attentions recently. Herein, p-type SnSe polycrystalline bulk materials with good thermoelectric properties are presented. By using the $SnSe_2$ nanostructures synthesized via a wet-chemistry route as the precursor, polycrystalline SnSe bulk materials were successfully obtained by a combined heat-treating process under reducing atmosphere and following spark plasma sintering procedure. As a reference, the SnSe nanostructures synthesized via a wet-chemistry route were also fabricated into polycrystalline bulk materials through the same process. The thermoelectric properties of the SnSe polycrystalline transformed from $SnSe_2$ nanostructures indicate that the increasing of heattreating temperature could effectively decrease the electrical resistivity, whereas the decrease in Seebeck coefficient is nearly invisible. As a result, the maximum power factor is enhanced from 5.06×10^{-4} W/m·K^2 to 8.08×10^{-4} W/m·K^2 at 612 °C. On the other hand, the reference sample, which was obtained by using SnSe nanostructures as the precursor, displays very poor power factor of only 1.30×10^{-4} W/m·K^2 at 537 °C. The x-ray diffraction (XRD), scanning electron microscope (SEM), x-ray fluorescence (XRF), and Hall effect characterizations suggest that the anisotropic crystal growth and existing Sn vacancy might be responsible for the enhanced electrical transport in the polycrystalline SnSe prepared by using $SnSe_2$ precursor. On the other hand, the impact of heat-treating temperature on thermal conductivity is not obvious. Owing to the boosting of power factor, a high zT value of 1.07 at 612 °C is achieved. This study provides a new method to synthesize polycrystalline SnSe and pave a way to improve the thermoelectric properties of polycrystalline bulk materials with similar layered structure.

Keywords: thermoelectric properties, $SnSe_2$ nanostructures, polycrystalline SnSe, anisotropic crystal growth

PACS: 72.20.Pa, 72.15.Jf, 72.80.Jc, 81.07.–b **DOI:** 10.1088/1674-1056/27/4/047211

1. Introduction

Thermoelectric materials are becoming more and more concerned, aiming at boosting their applications in waste-heat recovery and cooling.[1,2] Generally, the thermoelectric conversion efficiency can be determined by a figure of merit $zT = S^2\sigma T/\kappa$, where T, S, σ, and κ are absolute temperature, the Seebeck coefficient, electrical conductivity, and thermal conductivity of a thermoelectric material, respectively. Obviously, high zT is equivalent to high power factor ($S^2\sigma$) and low thermal conductivity simultaneously. In the past decade, several strategies were usually adopted to enhance the power factor of bulk materials, such as carrier concentration engineering,[3,4] increase of band degeneracy,[4–6] enhancement of band effective mass,[7,8] and improvement of carrier mobility.[9] To decrease the thermal conductivity, which contributes most significant advances in improving zT, there are several principles, including introducing point defects,[10] second-phase nanostructures,[11–13] all-length-scale hierarchical architectures,[14,15] and choosing compounds with complex crystal structures.[16]

In 2014, Zhao *et al*. reported that a record zT ~2.6 at 923 K was achieved along the b axis of SnSe single crystal, benefiting from the low lattice thermal conductivity (0.23 W/m·K at 973 K) which was mainly ascribed to large phonon anharmonicity.[17,18] Furthermore, enhanced power factor and ultrahigh average zT (1.60) in the range from 300 K to 923 K were realized in Na-doped samples.[4,6,19] These exciting phenomena have stimulated much interest on this selenide which consists of earth-abundant and environmentally friendly elements. However, the application of thermoelectric SnSe single crystals is hindered because their growth is challenging due to a strong phase transition at high temperature and machinability is poor owing to the weak chemical bonds along a axis. As a result, considerable effort has

*Project supported by the National Natural Science Foundation of China (Grant Nos. 51572049, 51562005, and 51772056), the Natural Science Foundation of Guangxi Zhuang Automomous Region, China (Grant Nos. 2015GXNSFFA139002 and 2016GXNSFBA380152), and the Open Fund of Key Laboratory of Cryogenics, Technical Institute of Physics and Chemistry, Chinese Academy of Sciences (Grant No. CRYO201703).

†Corresponding author. E-mail: miaolei@guet.edu.cn

© 2018 Chinese Physical Society and IOP Publishing Ltd

been focused on improving the thermoelectric performance of polycrystalline SnSe.[20–25] Unfortunately, up to date, the ultrahigh zT values of SnSe crystals have not been reproduced in polycrystalline SnSe because polycrystalline samples show lower carrier mobility and higher thermal conductivity. It is reasonable to suppose that the carrier scattering at grain boundaries and random distribution of crystalline grains with strong anisotropy should decrease the carrier mobility. Unexpectedly, the higher lattice thermal conductivity of polycrystalline SnSe is reported by lots of papers, which is at odds with the simple expectation that grain boundary scattering should act as an additional source of phonon scattering.[26] The possible oxidation in polycrystalline SnSe could reconcile this contradicting result since SnO has very high thermal conductivity (∼98 W/m·K).[27,28] Besides, vast off-stoichiometric defects[10] and relatively low density[29] may provide additional contribution to the ultralow lattice thermal conductivity.

To improve the thermoelectric performance of polycrystalline SnSe, Na,[30] K,[21,31] Ag,[22] Br,[23] I,[24] and $BiCl_3$[25] have all been proven to be effective dopants in both p-type and n-type samples. Nevertheless, the maximum zT nearly keeps at relatively low values (< 1.3) though the carrier concentration is effectively increased. SnSe crystallizes in a highly anisotropic layered orthorhombic (*Pnma* group) crystal structure below 800 K and undergoes a structural transition from *Pnma* to *Cmcm* above 800 K.[32,33] The layered structure suggests that the control of crystalline orientation is very significant in polycrystalline SnSe samples.[34,35] Besides, Sn vacancy always plays an important role in improving the thermoelectric properties because it resembles hole-doping which can enhance the carrier concentration of p-type SnSe by shifting the Fermi level and simultaneously inducing localized flat bands in the vicinity of the Fermi energy level.[36–38] Meanwhile, it also acts as point defect to scatter phonon and then decrease the thermal conductivity. These motivate us to optimize the thermoelectric properties by simultaneously regulating the anisotropic crystal growth and Sn vacancy.

In this study, the SnSe polycrystalline bulk materials were successfully prepared by heat treating the $SnSe_2$ nanostructures synthesized via a wet-chemistry route at temperature above 600 °C. $SnSe_2$ is a semiconductor with layered CdI_2-type structure, and has very strong anisotropic electrical and thermal properties.[39–42] This distinctive crystalline orientation of precursor $SnSe_2$ may affect the anisotropic crystal growth during the transformation of $SnSe_2$ to SnSe. Furthermore, vast Sn vacancy should be formed during this process because of the sublimation of atoms. In fact, the measurement of thermoelectric properties demonstrate that the intensified anisotropic crystal growth and Sn vacancy enhance the power factor from 5.06×10^{-4} W/m·K^2 to 8.08×10^{-4} W/m·K^2 at 612 °C. Then, a high zT value of 1.07 at 612 °C is obtained.

2. Experimental section

2.1. Chemical reagents

Tin chloride dihydrate ($SnCl_2 \cdot 2H_2O$, 99.99%), selenium dioxide (SeO_2), and hydrazine hydrate ($N_2H_4 \cdot H_2O$, 98%) were purchased from Aladdin industrial corporation, Shanghai, China. All the chemicals were analytical grade and used without purification.

2.2. Synthesis of $SnSe_2$ and SnSe nanostructures

The $SnSe_2$ and SnSe nanostructures were synthesized by a condensing reflux method. In a typical synthesis process of $SnSe_2$ nanostructures, 2.256 g of $SnCl_2 \cdot 2H_2O$ and 2.220g of SeO_2 were added into 250 ml of glycol with magnetic stirring in a 500-ml round bottom flask with three necks, which was heated by an oil-bath. Then 6-mL of $N_2H_4 \cdot H_2O$ was poured into the above solution when the temperature in glycol reaches 80 °C (Attention! A large amount of heat and gas (or foam) generated as soon as the hydrazine was added). After further increasing to the assigned temperature, the status of flask was maintained for 24 h in the oil-bath. In this experiment, the highest temperature in glycol would reach 182 °C (The solution was boiling). After the reaction, it was cooled down to room temperature naturally. The black powders were collected after washing using absolute ethanol and deionized water, and then dried under vacuum at 60 °C for 12 h. SnSe nanostructures were synthesized by the same process except that the molar ratio of Sn to Se was 1:1, namely 2.256 g of $SnCl_2 \cdot 2H_2O$ and 1.110 g of SeO_2.

2.3. Fabrication of the SnSe polycrystalline bulk materials

At first, the $SnSe_2$ and SnSe nanostructures synthesized via a wet-chemistry route were cold-pressed into cylinders with a diameter of 20 mm under a force of 9.8 kN. After the heat-treating process under mixed gases (8% H_2 + 92% Ar) for protecting the samples from oxidation at different temperatures for 15 h in a tubular furnace, the cylinders were grounded into powders again. The flow rate of protective gases was 0.15 L/min and the heating rate of tubular furnace was 5 °C/min. Then, the powders were fabricated into cylinders with a diameter of 20 mm again by a spark plasma sintering (SPS, LABOX-325, SINTER LAND INC.) method with a pressure of 50 MPa at 360 °C (for the samples whose heat-treating temperature was 400 °C and 500 °C) and 500 °C (for the other samples) for 6 min. The sintered samples from $SnSe_2$ nanostructures are identified by T@$SnSe_2$, where T is heat-treating temperature, while the samples from SnSe nanostructures corresponding to T@SnSe. Finally, prisms with the size of about 3 mm × 3 mm × 15 mm were cut from the sintered cylinders for the characterization of electrical resistivity and Seebeck coefficient, and wafers with a diameter of 10 mm and

5 mm were prepared for the measurement of thermal diffusivity and specific heat, respectively.

2.4. Characterization

The crystal structures of the powders and bulk materials were characterized by powder diffractometry (PANalytical X'pert Pro MPD operated at 40 kV and 40 mA, CuKa, $\lambda = 0.154$ nm). And their morphology observation was performed on a field-emission scanning-electron microscopy (FE-SEM; Hitachi S-4800, Japan) and transmission electron microscopy (TEM) (Tecnai G220). The composition was determined by x-ray fluorescence (XRF) analysis. Electrical resistivity (ρ) and Seebeck coefficient (S) were measured by the static DC method (ZEM-3; ULVAC RIKO, Japan) in a low-helium (99.999%) atmosphere with a temperature gradient from 20 °C to 30 °C and 40 °C. The thermal conductivity (κ) is calculated from $\kappa = D\rho C_{\mathrm{p}}$, where D is the thermal diffusivity, C_{p} is the specific heat, and ρ is the measured density. The thermal diffusivity (D) was measured by a laser flash method (LFA-457; NETZSCH); the specific heat was determined by differential scanning calorimetry (DSC) (DSC-404F3, NETZSCH); and the volume density (ρ) was determined by Archimedes' method. The Hall coefficient (R_{H}) at room temperature was measured in a Quantum Design, Inc. Physical Properties Measurement System (PPMS). The Hall carrier concentration (n) and mobility (μ) were evaluated by using the formula $R_{\mathrm{H}} = 1/ne$ and $\sigma = ne\mu$, respectively.

3. Results and discussion

In this experiments, the temperature of the condensing reflux method in solvent was regulated. After the reaction, black powders were obtained. The corresponding XRD patterns are shown in Fig. 1(a). From this figure, we could conclude that only peaks well-matched with Se (JCPDS 01-086-2246) are observed if the temperature does not exceed 100 °C. However, the XRD patterns of samples synthesized at temperatures above 100 °C could be indexed to $SnSe_2$ phase (JCPDS 01-089-2939) without any impure phase. Furthermore, the intensity of peaks becomes stronger and the corresponding full-width at half-maximum (FWHM) decreases with increasing reaction temperature. This result suggests that the elevated temperature activates the reaction and then increases the grain size of $SnSe_2$ nanostructures. Similarly, it is unable to obtain SnSe nanostructures at temperature below 110 °C as reflected by Fig. 1(b). Fortunately, the XRD patterns of powders obtained at the temperature above 110 °C could be ascribed to SnSe crystal structure (JCPDS 00-048-1224). No obvious peaks of impurities can be observed when the reaction temperature exceeds 140 °C, demonstrating the successful synthesis of SnSe nanostructures via this wet-chemistry method.

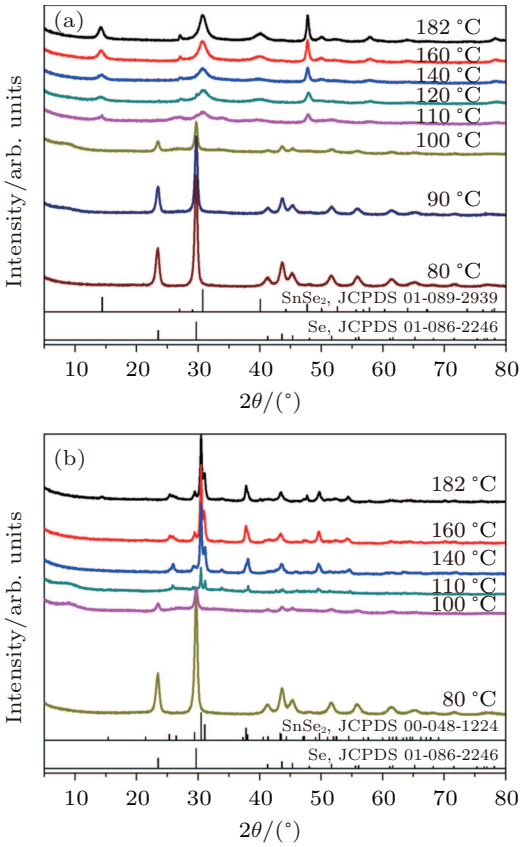


Fig. 1. (color online) XRD patterns of (a) $SnSe_2$ and (b) SnSe powders synthesized via a wet-chemistry route at different reaction temperatures.

The morphologies of the $SnSe_2$ and SnSe nanostructures were observed by SEM and TEM. As given in Fig. 2, the characterization of SEM shows that the $SnSe_2$ nanostructures obtained at 140 °C have the shape of nano-petal (Fig. 2(a)). On the other hand, the morphology of the sample synthesized at 182 °C looks more like potato chips with nanosize (Fig. 2(b)). Obviously, the increasing of reaction temperature increases the size of nanostructures, which is in accordance with the XRD results. In detail, the width of these two-dimensional nanostructures is expanded from nanometer (140 °C) to micrometer (182 °C). Though SnSe also has layered crystal structure, the SnSe nanostructures display agglomerated nanoparticles. Meanwhile, the sample obtained at 182 °C (Fig. 2(d)) presents larger agglomerations than that of the one prepared at 140 °C (Fig. 2(c)). Figure 3 shows the typical TEM and HRTEM images. In agreement with the observation of SEM, the $SnSe_2$ sample synthesized at 182 °C (Fig. 3(a)) reveals nanosheets with the thickness of several nanometers to about 50 nm and the width of several hundred nanometers to about 1.5 μm. In contrast, nanoparticles with the size of several nanometers to about 25 nm are absorbed on the surface of lumps in the SnSe sample obtained at 182 °C (Fig. 3(b)). The HRTEM characterization reconfirms the crystal structures of $SnSe_2$ and SnSe by matching the crystal plane spacing as shown in the insets of Figs. 3(a) and 3(b), respectively.

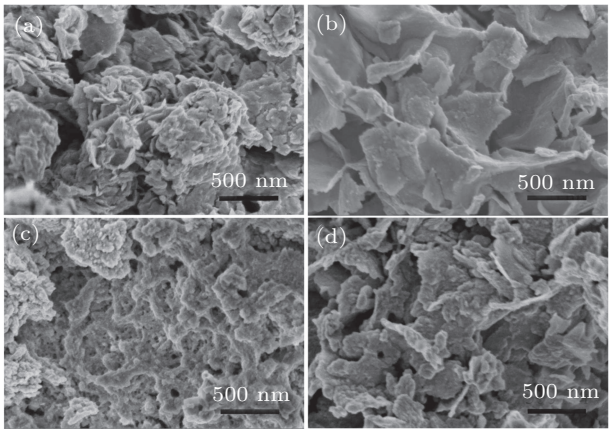


Fig. 2. SEM images of $SnSe_2$ and SnSe nanostructures synthesized at 140 °C [(a) and (c)] and 182 °C [(b) and (d)], respectively.

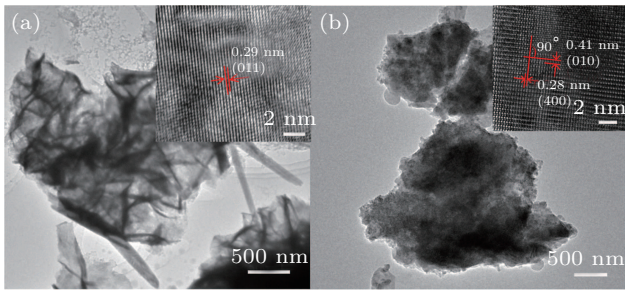


Fig. 3. (color online) TEM images of (a) $SnSe_2$ and (b) SnSe nanostructures synthesized at 182 °C. The insets are their corresponding HRTEM images.

We prepared the polycrystalline SnSe via two methods as described in Section 2. The only difference between them is the choice of precursors, namely $SnSe_2$ and SnSe nanostructures. The structure of the samples was investigated by XRD measurement. The collected patterns are given in Fig. 4 and demonstrate that the prepared $SnSe_2$ keeps its original crystal structure until the temperature of heat-treating is elevated to 550 °C, where some peaks indexed to SnSe phase (JCPDS 00-014-0059) appear. With further increasing the temperature, the precursor of $SnSe_2$ transforms into SnSe phase completely at 600 °C, without observable diffraction of impurities. Due to the higher vapor pressure of Se than that of Sn, it is anticipated that the sublimation of Se should be stronger than that of Sn, driving the formation of SnSe phase at high temperature (≥600 °C). When the temperature reaches 850 °C, a small amount of powders were collected in our experiments, which is not enough to fabricate bulk materials. Interestingly, the obtained SnSe phase indicates a strong anisotropic crystal growth, which is reflected by the fact that the diffraction intensity of (400) crystal face is particularly stronger than the others. The *bc* orientation degree for the (*h*00) crystal planes termed as *F* (*h*00) can be calculated with Lotgering method by the following equations[42]

$$F = \frac{P - P_0}{1 - P_0},$$

$$P_0 = \frac{I_0\,(h00)}{\sum I_0\,(hkl)},$$

$$P = \frac{I\,(h00)}{\sum I\,(hkl)},$$

where P and P_0 are the ratios of the integrated intensities of all (*h*00) crystal planes to those of all (*hkl*) planes for preferentially and randomly oriented samples, respectively. $F = 0$ and $F = 1$ mean completely disordered and ordered, respectively. In the present work, the P and P_0 are calculated by using the XRD data and the standard card (JCPDS No. 00-014-0159). The result indicates that the $F_{(h00)}$ values are 0.51, 0.76, and 0.89 for the XRD patterns of the samples with heat-treating temperature of 600 °C, 700 °C, and 800 °C, respectively. This improved anisotropic crystal growth along *bc* plane should be beneficial to improving the thermoelectric properties since the direction along *b* axis has the best thermoelectric performance.[17] Oppositely, the strongest diffraction peak of the samples prepared by using SnSe nanostructures as the precursor could be ascribed to (111) crystal face, which is typically shown in the inset in Fig. 4.

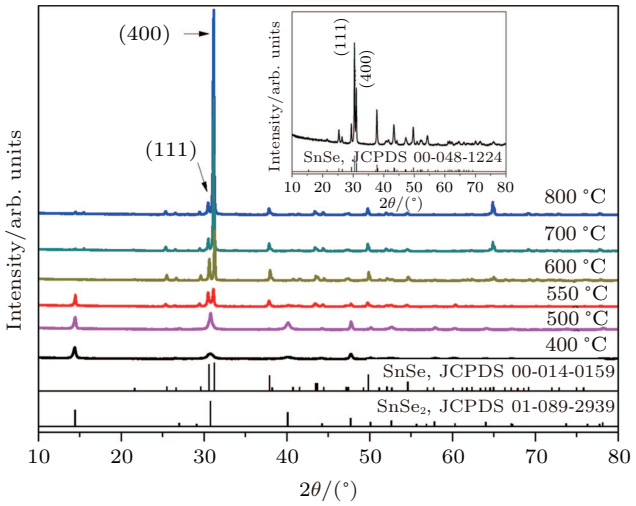


Fig. 4. (color online) XRD patterns of the polycrystalline obtained by treating the precursors of $SnSe_2$ nanostructures in a tubular furnace at different temperatures. The inset is the XRD patterns of the reference, which prepared by using SnSe nanostructures as the precursor.

The phenomena of anisotropic crystal growth are also affirmed by the SEM observation, which was performed on the fracture surface parallel to the pressing direction of the SPS process. Figures 5(a)–5(c) give the images of the sample 400 °C@$SnSe_2$, 600 °C@$SnSe_2$, and 800 °C@$SnSe_2$, respectively. Apparently, all samples show a layered morphology. Meanwhile, the size of slice becomes larger and larger with increasing the temperature. This is reasonable because that both $SnSe_2$ and SnSe have a layered structure. However, as shown in Fig. 5(d), the anisotropic crystal growth of the sample 600 °C@SnSe is weaker.

Figure 6 displays the thermoelectric properties being measured perpendicular to the pressing direction of the SPS process, which present a better thermoelectric performance

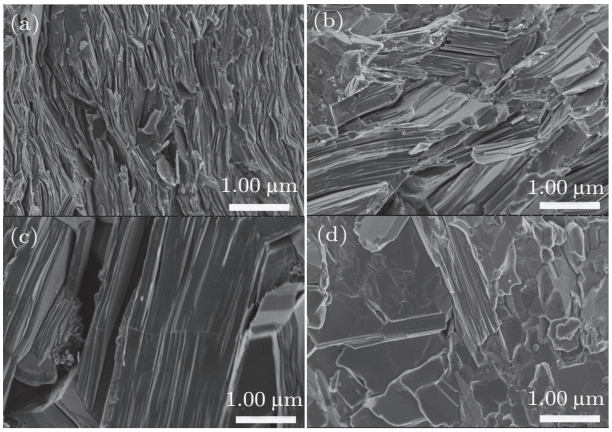


Fig. 5. (color online) SEM images of the fracture surface parallel to the pressing direction of SPS process: (a) 400 °C@$SnSe_2$, (b) 600 °C@$SnSe_2$, (c) 800 °C@$SnSe_2$, and (d) 600 °C@SnSe.

than those being measured the parallel to the pressing direction in our experiment. In Fig. 6(a), we find that the electrical resistivity increases gradually at temperature ranging from 50 °C to about 300 °C, and then decreases sharply at temperature ranging from 300 °C to about 550 °C for the SnSe bulk materials prepared by using $SnSe_2$. Meanwhile, the increasing of the heat-treating temperature decreases the electrical resistivity from 2.26×10^{-4} Ω·m (600 °C) to 1.38×10^{-4} Ω·m (800 °C) at about 612 °C. This phenomenon may be mainly owing to the increased grain size as observed by SEM, which should improve the carrier mobility due to the decreased carrier scattering at grain boundaries. On the other hand, the sample 600 °C@SnSe has higher electrical resistivity. Generally, the electrical conductivity is determined by the carrier

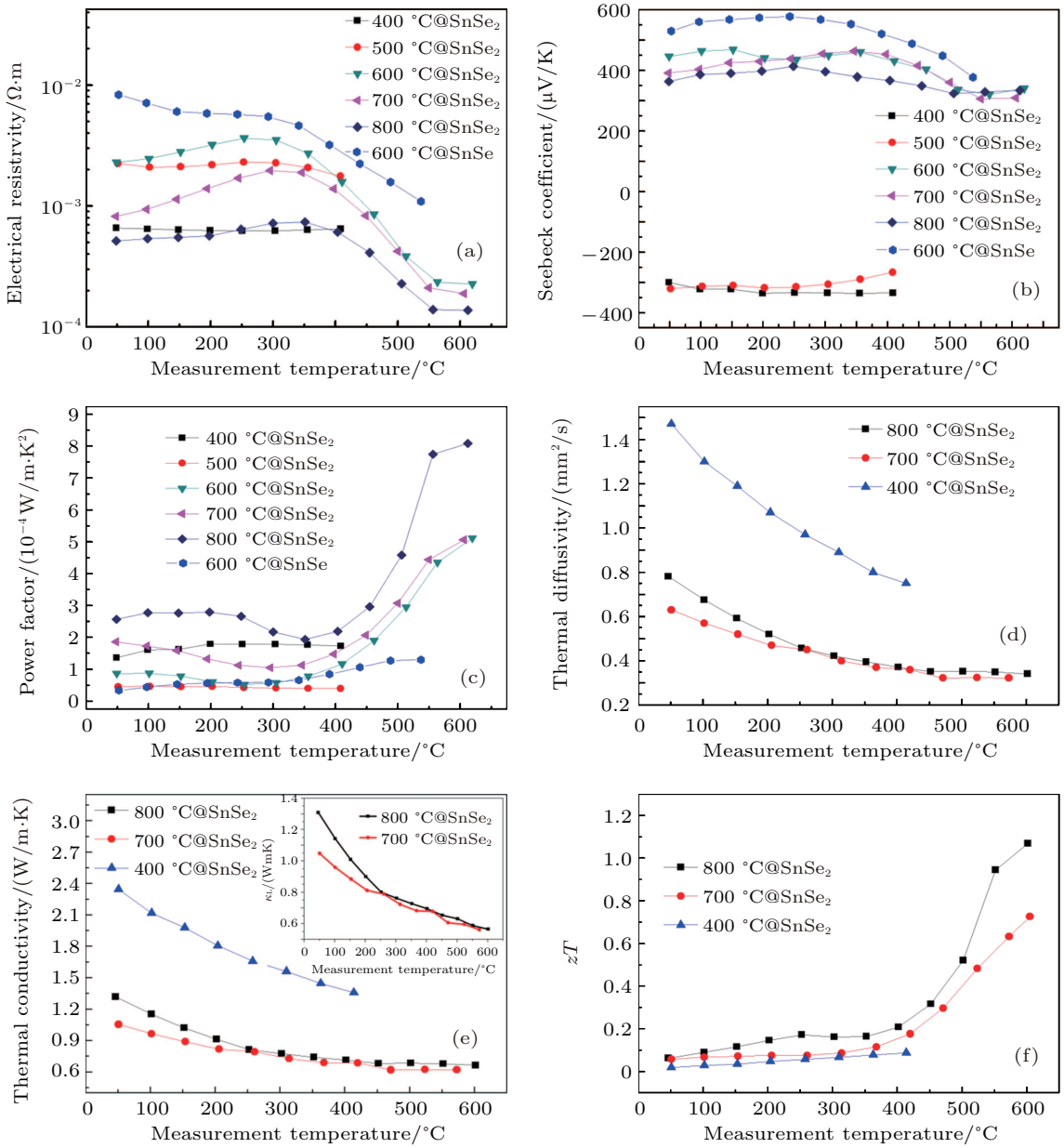


Fig. 6. (color online) Thermoelectric properties of the polycrystalline along the orientation perpendicular to the pressing direction of SPS process: (a) electrical resistivity, (b) Seebeck coefficient, (c) power factor, (d) thermal diffusivity, (e) thermal conductivity (κ_T), and (f) zT. The inset in panel (e) is the lattice thermal conductivity (κ_l), which is calculated based on $\kappa_l = \kappa_T - \kappa_e$. The carrier thermal conductivity (κ_e) is estimated based on the Wiedemann–Franz law ($\kappa_e = L\sigma T$). The Lorenz number is derived from Fermi energy with a simple one-band model and only acoustic phonon scattering considered.

concentration and mobility according to the formula $\sigma = ne\mu$. Therefore, anisotropic crystal growth in polycrystalline SnSe along *bc* plane would favor the transport of carriers because the carrier mobility in SnSe crystals is higher along *b* and *c* axes than that of *a* axis. Based on the observation of SEM, which shows that the sample 600 °C@SnSe has weaker anisotropic crystal growth than the others, it is easy to anticipate that the carrier mobility in sample 600 °C@SnSe would be lower. Besides, it is reasonable to conclude that the sample *T*@$SnSe_2$ contains more Sn vacancy than *T*@SnSe, since the former (1.12/1) has a higher n_{Se}/n_{Sn} value than that of the latter one (1.03/1) as shown in Table 1. Usually, Sn vacancy could provide holes,[34] and then both the increased carrier mobility and concentration in sample *T*@$SnSe_2$ would decrease the electrical resistivity. The evaluated Hall concentration and mobility at room temperature as shown in Table 2 also agree well with the above conclusion as follows. The sample 600 °C@$SnSe_2$ (8.45×10^{17} cm^{-3}, 32.4 $cm^2/V{\cdot}s$) owns higher carrier concentration and mobility than the sample 600 °C@SnSe (7.02×10^{17} cm^{-3}, 21.6 $m^2/V{\cdot}s$), suggesting that the precursor of $SnSe_2$ nanostructures is more beneficial for the generation of Sn vacancy and anisotropic crystal growth. At the same time, the elevated heat-treating temperature may also enhance the formation of Sn vacancies and anisotropic crystal growth since the carrier concentration and mobility are improved to 4.81×10^{18} cm^{-3} and 36.4 $cm^2/V{\cdot}s$ for the sample 800 °C@$SnSe_2$, respectively. The Seebeck coefficient measurement given in Fig. 6(b) shows that $SnSe_2$ bulk materials have negative values, suggesting that they are n-type semiconductors, while polycrystalline SnSe bulk materials presents positive values, reflecting their p-type properties. This is consistent with the results in earlier reports.[34,40] Besides, the Seebeck coefficient depending on the heat-treating temperature varies limitedly. For example, the Seebeck coefficient of the sample 800 °C@$SnSe_2$ is 334 μV/K while that of the sample 700 °C@$SnSe_2$ is 340 μV/K at 612 °C. In line with the trend of electrical resistivity, the Seebeck coefficient of the sample 600 °C@SnSe is reasonably higher. However, because of its higher electrical resistivity, the sample 600 °C@SnSe shows very low power factor as revealed in Fig. 6(c), only 1.30×10^{-4} $W/m{\cdot}K^2$ at 537 °C. In the samples *T*@$SnSe_2$, thanks to the remarkably improved electrical transport, the power factor is enhanced from 5.06×10^{-4} $W/m{\cdot}K^2$ to 8.09×10^{-4} $W/m{\cdot}K^2$ at 612 °C, which is comparable with the single crystal.[17] The thermal diffusivity and thermal conductivity are shown in Figs. 6(d) and 6(e), respectively. From these figures, it is easy to conclude that the thermal transport in SnSe is more difficult than that in $SnSe_2$. For instance, in comparison with the sample 800 °C@$SnSe_2$ (1.32 W/mK), the thermal conductivity of the sample 400 °C@$SnSe_2$ is almost twice at 51 °C (2.34 W/m·K) . As shown in the inset of Fig. 6(e), the lattice thermal conductivity of the sample 700 °C@$SnSe_2$ locates only a little bit below that of the sample 800 °C@$SnSe_2$ above 300 °C. Meanwhile, the thermal conductivity of the sample 800 °C@$SnSe_2$ is also relatively low, only 0.66 W/m·K at 612 °C. As a result of the greatly improved power factor and relatively low thermal conductivity, a maximum zT value of 1.07 at 612 °C is obtained by the sample 800 °C@$SnSe_2$. To the best of our knowledge, it is one of the best results of SnSe polycrystalline samples without foreign-atomic doping.

Table 1. The chemical composition of the polycrystalline samples obtained by XRF measurement.

Sample	Mass fraction of Se/%	Mass fraction of Sn/%	Chemical fomula
400 °C@$SnSe_2$	53.75616	41.09509	$SnSe_{1.97}$
800 °C@$SnSe_2$	41.11609	55.34402	$SnSe_{1.12}$
600 °C@SnSe	38.94319	56.97995	$SnSe_{1.03}$

Table 2. The carrier concentration and Hall mobility of the polycrystalline samples.

Sample	Carrier concentration/cm^{-3}	Hall mobility/($cm^2/V{\cdot}s$)
800 °C@$SnSe_2$	4.81×10^{18}	36.4
600 °C@$SnSe_2$	8.45×10^{17}	32.4
600 °C@SnSe	7.02×10^{17}	21.6

4. Conclusion

In this study, by using $SnSe_2$ nanostructures as the precursor, polycrystalline SnSe was successfully prepared by a combined heat-treating process in a reducing atmosphere and following spark plasma sintering procedure It shows better thermoelectric properties than that of the reference sample 600 °C@SnSe. Owing to the reduction of electrical resistivity, the power factor is enhanced from 5.06×10^{-4} $W/m{\cdot}K^2$ to 8.08×10^{-4} $W/m{\cdot}K^2$ at 612 °C. XRD, SEM, XRF, and Hall effect characterizations suggest that anisotropic crystal growth and Sn vacancy may be responsible for the enhanced electrical transport. In addition, the thermal conductivity has a weak relationship with the heat-treating temperature As a result, a high zT value of 1.07 at 612 °C is achieved, which is one of the best results of SnSe polycrystalline samples without foreign-atomic doping. This study provides a new method to synthesize polycrystalline SnSe and pave a way to improve the thermoelectric properties of polycrystalline bulk materials with similar layered structure.

References

[1] Liu W, Jie Q, Kim S H and Ren Z 2015 *Acta Mater.* **87** 357

[2] Alam H and Ramakrishna S 2013 *Nano Energy* **2** 190

[3] Pei Y, Gibbs Z M, Gloskovskii A, Balke B, Zeier W G and Synder G J 2014 *Adv. Energy Mater.* **4** 1400486

[4] Zhao L D, Tan G, Hao S, He J, Pei Y, Chi H, Wang H, Gong S, Xu H, Dravid V P, Uher C, Snyder G J, Wolverton C and Kanatzidis M G 2016 *Science* **351** 141

[5] Pei Y, Shi X, LaLonde A, Wang H, Chen L and Snyder G J 2011 *Nature* **473** 66

[6] Peng K, Zhang B, Wu H, Cao X, Li A, Yang D, Lu X, Wang G, Han X, Uher C and Zhou X 2017 *Mater. Today*

[7] Heremans J P, Jovovic V, Toberer E S, Saramat A, Kurosaki K, Charoenphakdee A, Yamanaka S and Snyder G J 2008 *Science* **321** 554

[8] Tan G, Zhao L D and Kanatzidis M G 2016 *Chem. Rev.* **116** 12123

[9] Zhang X, Liu J, Li Y, Su W B, Li J C, Zhu Y H, Li M K, Wang C M and Wang C L 2015 *Chin. Phys. Lett.* **32** 037201

[10] Wu D, Wu L, He D, Zhao L D, Li W, Wu M, Jin M, Xu J, Jiang J, Huang L, Zhu Y, Kanatzidis M G and He J 2017 *Nano Energy* **35** 321

[11] Cao B L, Jian J K, Ge B H, Li S M, Wang H, Liu J and Zhao H Z 2017 *Chin. Phys. B* **26** 017202

[12] Minnich A J, Dresselhaus M S, Ren Z F and Chen G 2009 *Energy Environ. Sci.* **2** 466

[13] Wu Z H, Xie H Q, Zhai Y B, Gan L H and Liu J 2015 *Chin. Phys. B* **24** 034402

[14] Zhao L D, Dravid V P and Kanatzidis M G 2014 *Energy Environ. Sci.* **7** 251

[15] Biswas K, He J, Blum I D, Wu C I, Hogan T P, Seidman D N, Dravid V P and Kanatzidis M G 2012 *Nature* **489** 414

[16] Kleinke H 2010 *Chem. Mater.* **22** 604

[17] Zhao L D, Lo S H, Zhang Y, Sun H, Tan G, Uher C, Wolverton C, Dravid V P and Kanatzidis M G 2014 *Nature* **508** 373

[18] Li C W, Hong J, May A F, Bansal D, Chi S, Hong T, Ehlers G and Delaire O 2015 *Nat. Phys.* **11** 1063

[19] Peng K, Lu X, Zhan H, Hui S, Tang X, Wang G, Dai J, Uher C, Wang G and Zhou X 2016 *Energy Environ. Sci.* **9** 454

[20] Fu J, Su X, Xie H, Yan Y, Liu W, You Y, Cheng X, Uher C and Tang X 2018 *Nano Energy* **44** 53

[21] Ge Z H, Song D, Chong X, Zheng F, Jin L, Qian X, Zheng L, Dunin-Borkowski R E, Qin P, Feng J and Zhao L D 2017 *J. Am. Chem. Soc.* **139** 9714

[22] Chere E K, Zhang Q, Dahal K, Cao F, Mao J and Ren Z 2016 *J. Mater. Chem. A* **4** 1848

[23] Zhang Q, Chere E K, Sun J, Cao F, Dahal K, Chen S, Chen G and Ren Z 2015 *Adv. Energy Mater.* **5** 1500360

[24] Chang C, Tan Q, Pei Y, Xiao Y, Zhang X, Chen Y X, Zheng L, Gong S, Li J E, He J and Zhao L D 2016 *RSC Adv.* **6** 98216

[25] Wang X, Xu J, Liu G, Fu Y, Liu Z, Tan X, Shao H, Jiang H, Tan T and Jiang J 2016 *Appl. Phys. Lett.* **108** 083902

[26] Ibrahim D, Vaney J B, Sassi S, Candolfi C, Ohorodniichuk V, Levinsky P, Semprimoschnig C, Dauscher A and Lenoir B 2017 *Appl. Phys. Lett.* **110** 032103

[27] Zhao L D, Chang C, Tan G and Kanatzidis M G 2016 *Energy Environ. Sci.* **9** 3044

[28] Zhang B, Peng K, Sha X, Li A, Zhou X, Chen Y, Deng Q, Yang D, Ma E and Han X 2017 *Microsc. Microanal.* **23** 173

[29] Wei P C, Bhattacharya S, He J, Neeleshwar S, Podila R, Chen Y Y and Rao A M 2016 *Nature* **539** E1

[30] Wei T R, Tan G J, Zhang X, Wu C F, Li J F, Dravid V P, Snyder G J and Kanatzidis M G 2016 *J. Am. Chem. Soc.* **138** 8875

[31] Chen Y X, Ge Z H, Yin M J, Feng D, Huang X Q, Zhao W Y and He J Q 2016 *Adv. Funct. Mater.* **26** 6836

[32] Chattopadhyay T, Pannetier J and Vonschnering H G 1986 *J. Phys. Chem. Solids* **47** 879

[33] Asfandiyar, Li Z L, Sun F H, Pan Y, Wu C F, Farooq M U, Tang H C, Li F, Li B, Li J F and Wei T R 2017 *Sci. Rep.* **7** 43262

[34] Wang X, Xu J, Liu G Q, Tan X, Li D, Shao H, Tan T and Jiang J 2017 *NPG Asia Mater.* **9** e426

[35] Popuri S R, Pollet M, Decourt R, Morrison F D, Bennett N S and Bos J W G 2016 *J. Mater. Chem. C* **4** 1685

[36] Wei W, Chang C, Yang T, Liu J, Tang H, Zhang J, Li Y, Xu F, Zhang Z, Li J F and Tang G 2018 *J. Am. Chem. Soc.* **140** 499

[37] Dewandre A, Hellman O, Bhattacharya S, Romero A H, Madsen G K H and Verstraete M J 2016 *Phys. Rev. Lett.* **117** 276601

[38] Liu C, Miao L, Hu D, Huang R, Fisher C A J, Tanemura S and Gu H 2013 *Phys. Rev. B* **88** 205201

[39] Saha S, Banik A and Biswas K 2016 *Chem. Eur. J.* **22** 15634

[40] Luo Y, Zheng Y, Luo Z, Hao S, Du C, Liang Q, Li Z, Khor K A, Hipalgaonkar K, Xu J, Yan Q, Wolverton C and Kanatzidis M G 2017 *Adv. Energy Mater.* 1702167

[41] Xu P, Fu T, Xin J, Liu Y, Ying P, Zhao X, Pan H and Zhu T 2017 *Sci. Bull.* **62** 1663

[42] Li F, Zheng Z, Li Y, Wang W, Li J F, Li B, Zhong A, Luo J and Fan P 2017 *J. Mater. Sci.* **52** 1